Retrieving Scale from Quasi-Stationary Images

Piotr W. Mirowski[1] and Daniel M. Tetzlaff[2]

1 - Courant Institute of Mathematical Sciences, New York University, 719 Broadway, 12th Floor, New York, NY 10003, USA, tel.: +1 203 278 1803, fax: +1 212 995 4122, piotr.mirowski@computer.org

2- Schlumberger Information Solutions, 5599 San Felipe, Suite 1700, Houston, TX 77056, USA, tel.: +1 713 513 2182, DTetzlaff@slb.com

The research work described in this article was done at Schlumberger-Doll Research, 320 Bent Street, Boston, MA 02141, USA, tel.: +1 617 252 4700.

Abstract (204 words)

We have developed a novel method to derive scale information from quasi-stationary images, which relies on a rotation-guided multi-scale analysis of features derived from Gray Level Co-occurrence Matrices (GLCM). Unlike other methods for multi-scale texture characterization, our method does not require rotation-invariant textural features, but instead uses orientation information derived from the image to constrain the algorithm. Our method computes GLCM textural features on a "stencil" that follows the local orientation field. It compares features obtained from a sliding window that scans the whole image with those present on a user-selected reference pattern. The method then calculates a similarity measure between textural features derived from the whole image and those derived from the reference pattern. By applying different affine transforms to the stencil used for sampling the reference pattern, we are able to measure the similarity between regions of the image and different dilated versions of the reference pattern, and hence perform a multi-resolution analysis of the image. For a given region of an image, our method is able to find the most likely scale. Therefore it can estimate the stationarity of the image in terms of scale, which has important applications to Multipoint Geostatistics. We tested the method on the Brodatz textures database.

Abstract (42 words)

Our novel multi-scale, rotation-guided algorithm derives scale information from quasi-stationary images. It extends Gray Level Co-Occurrence Matrices with variable size, oriented, image-sampling "stencils", and relies on similarity measures between reference patterns and the full image. It achieves successful applications to Multipoint Geostatistics.

Keywords:

Multi-scale; Rotation-guided; Texture Characterization; Gray-Level Co-occurrence Matrices; Quasi-stationary Images

Classification codes: 4.001, 4.001, 8.011

Abbrevations:

CNS: Circular Neighborhood System

GLCM: Gray-Level Co-occurrence Matrices

MPGS: Multipoint Geostatistics

1. Introduction

An image is stationary when all its spatial statistics are translation invariant. Stationarity is a property of the model assumed to have generated an image, rather than of a single image by itself. However, stationarity can be assessed from a single image in the same sense that the parameters of a statistical distribution can be assessed from a sample, namely by using certain measures of the sample that approximate the desired parameters, or that can be used as indicators of whether a certain hypothesis about the distribution may be true. As part of our work, we developed a set of measures of an image that would allow us to estimate three narrower aspects of stationarity that jointly provide a good assessment of overall stationarity (Caers, 2003): (a) stationarity of color or value (i.e. the requirement that the statistical distribution of pixel values is location independent), (b) stationarity of orientation (i.e. the requirement that local directional statistical properties –such as predominant correlation direction caused by similar orientation of repetitive shapes in the image- are location independent), and (c) stationarity of scale (the requirement that spatial variability -as manifested for example by the size of repetitive shapes that are present in the image- is location independent). The latter (scale stationarity) is the focus of this report. Many natural images exhibit a repetition of shapes with some variations in color, orientation, and scale, for instance images of a folded fabric, of a weaved basket, or aerial photographs of geological features such as alternations of river channels or sand dunes. Because we can only assess or estimate but not strictly prove the stationarity of these images, we loosely attribute the property of "quasi-stationarity" to them.

An interesting application for earth sciences is the retrieval of scale variations on textured images of geological bodies. Our research was prompted in particular by the stationarity requirements of a set of algorithms used in geology, called Multiple Point Geostatistics (MPGS). MPGS are a family of interpolation algorithms used to generate conditional simulations of geological property maps (Caers 2003). To a certain extent, MPGS resemble synthetic texture-generation algorithms. Starting from a so-called "training image", MPGS stochastically generate 2D maps (images) or 3D volumes reproducing their patterns. These algorithms are constrained by physical data (for instance derived from seismic acquisitions), and affinity (rotation and scale) property maps. One of the MPGS algorithm, SNESIM, can be summarized as following: 1) measure, on a training image, multivariate joint-statistics of pixel intensities, by scanning a "stencil" over the training image, and 2) stochastically generate the output image using these statistics, after possibly 2a) rescaling and 2b) rotating the generating stencil according to the corresponding rotation and scale property maps (Caers and Zhang, 2004, Tetzlaff et al., 2005).

Current state-of-the-art MPGS have statistical requirements for training images. Mainly, a valid training image should have the property of stationarity, which can consist of, but is not limited to, color distribution stationarity, orientation stationarity, and scale stationarity, as defined above. No method has yet been provided to verify scale stationarity of images used in MPGS. In this article we propose a method for the estimation of scale fields and scale stationarity of images. Our results in Section 4 explain how our scale stationarity estimations help in validating training images for MPGS.

Signal processing and statistical methods are two popular approaches to retrieve textural features. A first example of signal processing algorithms is a combination of scale and rotation filters such as the Gabor filter bank (Manjunath and Ma, 1996a, 1996b). For the Gabor filter, increasing the scale of analysis is equivalent to dilating the Gabor mother wavelet. Manjunath and Ma suggest a Gabor filter bank of 4 scales and 6 orientations for capturing complex texture features (Manjunath and Ma, 1996b). Other examples of signal processing algorithms rely on the 2D wavelet transform using other wavelet bases (Mallat, 1998). Among statistical methods is the Gray-Level Co-occurrence Matrices algorithm (GLCM), which computes second-order statistics on gray-level intensity of couples of pixels at various displacements (Bradley et al., 1995; Clausi, 2002; Haralick et al., 1973; Materka and Strzelecki, 1998; Visa, 1990). Bradley et al. (1995) suggest using the continuously varying displacement of the co-occurrence matrices as a continuously varying scale factor σ.

The main limitation of classical GLCM multi-scale texture classification algorithms is that they use the scale information to discriminate between patterns and do not assume that a pattern could occur at different scales. Therefore, two similar patterns reproduced at different scales on the image will be considered different patterns. Metzler et al. overcome the resolution-dependent quantification of textures by measuring cross-scale occurrences of gray level pairs instead of the more common co-occurrence gray level pairs. The multi-scale analysis is performed on filtered and scaled copies of the initial image (Metzler et al., 2000). However, our method aims at discriminating between scales; therefore we will take advantage of the scale dependency of GLCM.

A frequent problem with multi-scale image classification is that the discrimination between textures is based on scale and orientation information simultaneously, which means that two areas of an image having similar textures but different orientations will be classified as two different objects. This would be particularly limiting for geological applications, since patterns of interest to MPGS typically replicate similar textures with changing orientations. For this reason, we cannot use the basic implementations of GLCM or spectral descriptors such as 2D wavelet transform or Gabor filtering, since they are not rotation-invariant.

One approach to overcome varying orientation across the image consists of enhancing spectral methods using rotation-invariant texture features. For instance, Gaussian Markov Random Field or 2D Wavelet Packet features extracted from directional textures can be averaged over all directions (Deng and Clausi, 2004, Manthalkar et al, 2003). Alternatively, Gabor or Fourier texture feature vectors can be circularly shifted as a means to rotate a given pattern (Zhang, 2000, Arivazhagan et al., 2006, Huang and Aviyente, 2006). Similarly, Local Binary Patterns (Ojala et al., 2002) are a computationally simple rotation-invariant texture classification algorithm.

Our own approach is inspired by an MPGS algorithm where rotation-and-scale-dependent statistics are sampled on the training image, and then rotation and scale property maps guide the stochastic generation of an output image from the above statistics. We propose here a method that locally guides the orientation of a stencil that samples rotation-and-scale-dependent image statistics, and then takes advantage of the scale-specificity of that stencil to discriminate among various scales across the image.

Unlike other methods for multi-scale texture characterization that we are aware of, our method does not rely on rotation-invariant textural features, but takes advantage of the computed local image orientation field (local dominant direction) and uses rotation-dependent textural descriptors. We assume that we are able to obtain satisfactory estimates of the local orientation field from images using an algorithm based on the principal component of the local image gradient (Randen et al., 2000). Our original approach consists of using the local image orientation field to constrain the texture feature retrieval and then using texture descriptors that follow the local direction field. Once the texture descriptor is aligned with the local orientation, it can retrieve textural features organized in a more complex orientation distribution, e.g. with features mostly along one dominant direction but also along several other directions of smaller importance. The dominant direction corresponds to the local orientation field.

We decided to enhance the GLCM method for extraction of multi-scale textural features and make it rotation-guided. Although quite efficient in multi-scale texture classification, GLCM have proven not to perform as well as other techniques such as Gabor wavelets and filter banks or optimally designed Finite Impulse Response filter banks (Randen and Husoy, 1999). However, we retained this technique because of the analogy to multivariate joint statistics on pixel intensities used in MPGS (Caers, 2003). MPGS computes rotation and scale-dependent joint statistics on pixel intensities of a texture, then generates new textures from those statistics. MPGS methods can be constrained by local orientation and scale information (Caers and Zhang, 2004). Our GLCM-based method takes an inverse approach: it estimates the local orientation, locally rotates the "stencil" used to calculate GLCM second-order texture statistics, and finally discriminates between changes of scale to measure scale invariance across the image.

We explain the details of our rotation-guided GLCM algorithm in Section 2, then its applications to scale analysis in Section 3, and show the results obtained with three different datasets in Section 4. The first, simplistic one consists of synthetic chirp images (Sagiv et al, 2006, Pattichis and Bovik, 2007), and is destined to verify our scale retrieval algorithm. The second dataset is the Brodatz image database which enables us to evaluate the algorithm on natural photographs. Finally, we apply our algorithm to a set of MPGS training images.

2. Multi-resolution analysis of an image using a reference pattern

The general outline of our novel method can be summarized as follows (see Fig. 1): (a) extraction of a "reference pattern" from the image (section 2.1), (b) computation of the local directional field on the image (section 2.4), (c) orientation-controlled sampling of the image using Circular Neighborhood Systems (CNS, sections 2.3 and 2.4) and application of scale transforms to CNS (section 2.5), (d) extraction of textural features using Gray-Level Co-Occurrence Matrices (GLCM, section 2.2), and (e) comparison, at various scales, between GLCM vectors from the scaled reference pattern with GLCM vectors from other samples of the image (section 2.1).

2.1. Comparison of textural features between a reference pattern and samples of the image

The principle of the multi-resolution analysis scheme that we present in this article is basically similar to the well-known discrete wavelet analysis of a 2-D signal. In the latter, the image is "scanned" or analyzed by means of different wavelets derived from dilations of a mother 2-D wavelet, and the amplitude of the response for each wavelet is recorded as an image of wavelet coefficients (Mallat, 1998).

Here, the mother wavelet is replaced by a sample of the image called the "reference pattern". The quasi-stationarity assumption requires that the reference pattern be repeated at least twice along each dimension. In other words, the reference pattern needs to be small enough to be repeated across the image. Concurrently, sampling textural information from a large reference area enables to better capture the distribution of textural features of the whole image. Therefore, a larger reference area is more representative of the whole image. As a tradeoff between the repetition of the pattern and its complexity, we chose the size of the reference pattern to be at most 1/4 of the total image area. The reference pattern can be either picked by the user, or selected automatically in one of the 9 overlapping zones, covering each quarter of the image and illustrated on Fig. 2.

In order to perform a multi-resolution analysis of the image, instead of computing the convolution of the reference pattern with samples of the image, in our approach we compare the Euclidian distance between two vectors $F_{0,ax,ay}$ and $F_{1,x,y}$. Those vectors, which have the same number of elements N, contain textural features derived using GLCM (as explained in subsection 2.2). The first vector $F_{0,ax,ay}$ contains textural features computed over the reference pattern at a given scale $\mathbf{a}=(a_x,a_y)$. a_x is the scale factor along the X axis and a_y is the scale factor along the Y axis. The second vector $F_{1,x,y}$ contains features computed over a small sliding window extracted from the image. This sliding window is regularly sampled over the image at locations (x,y). The sliding window is of similar size to the reference pattern and has scale factors $\mathbf{a}=(a_x,a_y)=(1,1)$. We compute the similarity measure for different locations of the sliding window yielding $F_{1,x,y}$ (we "scan" the image) and also for different scale transforms of the reference pattern yielding $F_{0,sx,sy}$. We minimize the Euclidian distance between the textural-feature vectors $F_{0,ax,ay}$ and $F_{1,x,y}$ in order to estimate the scale $\mathbf{a}(x,y)$ of a sample of the image located at (x,y):

$$\mathbf{a}(x,y) = \underset{ax,ay}{\arg\min}\left(\sum_{i=1}^{N} \left[F_{1,x,y}(i) - F_{0,ax,ay}(i) \right]^2 \right). \tag{1}$$

Our full method, explained throughout Section 2, is illustrated on Fig. 1. We use orientation-controlled sampling to derive $F_{1,x,y}$ from GLCM of sliding window samples of the image and scale-and-rotation-controlled sampling to derive $F_{0,ax,ay}$ from GLCM of a bank of dilated versions of the reference pattern. Both sampling methods, as well as the derivation of the orientation field of the image, similarity maps, scale-space images and scale stationarity scores are explained in further subsections.

Because training images for MPGS are generally aerial photographs or images of geological outcrop analogs, scale variations of particular geological textures within an image are relatively limited in amplitude. Therefore we consider in the rest of our study scale variations up to a factor of 2. Moreover, geologists using MPGS are more interested in a global measure of scale variation over the whole image, rather than a precise scale estimate for each area of the image. We therefore use a discrete set of scales in our multi-resolution analysis: N_x=7 and N_y=7 scale factors $\{1/2,\ 2/3,\ 3/4,\ 1,\ 4/3,\ 3/2,\ 2\}$ for each dimension, with a total of 7×7=49 scales. Unlike the wavelet analysis, the reference pattern and its different dilations do not constitute an orthogonal basis.

2.2. Gray-Level Co-Occurrence Matrices (GLCM)

GLCM are a second-order method for measuring gray level textures in an image $I(x, y)$ (Materka and Strzelecki, 1998). The co-occurrence matrix $C_{\mathbf{d}}(i, j)$ describes the probability for gray levels i and j to occur in a given texture at a displacement of $\mathbf{d} = (x'-x, y'-y)$. For a given displacement $\mathbf{d}$, each element of the co-occurrence matrix is defined by:

$$C_d(i,j) = \Pr\left[I(x,y) = i, I(x',y') = j \,\middle|\, (x'-x, y'-y) = \mathbf{d} \right] + \Pr\left[I(x,y) = j, I(x',y') = i \,\middle|\, (x'-x, y'-y) = \mathbf{d} \right]. \tag{2}$$

Displacements can also be expressed in polar coordinates (r,θ). GLCMs are often computed in the literature on sets of displacements (or "stencils") consisting of a rigid set of radii such as r=1, 2, 3, etc. and angles $\theta = 0°, 45°, 90°, 135°$ (Bradley et al., 1995; Metzler et al., 2000; Visa, 1990). By our design, GLCMs are symmetric, which justifies our semi-circular sampling coverage (Materka and Strzelecki, 1998).

GLCMs are constructed by first quantizing an image into G gray levels, G often having in the literature a value of 32 or 64 for gray level images (Clausi, 2002). When performing a multi-resolution analysis of black and white patterns, we still resort to at least 32 gray levels, since during the scale and orientation transformations, pixel gray level values are often interpolated.

The content of GLCMs is characterized using content descriptors that extract statistics from the matrices. Haralick et al. (1973) defined various GLCM descriptors and we use 9 of them: energy (angular second moment), contrast (inertia), dissimilarity (absolute value), inverse difference, entropy, maximum probability, homogeneity, correlation, and variance.

GCLM features are computed for each displacement and then grouped into feature vectors. Typically, using 9 GLCM features and 28 displacements as in Fig. 3, we get feature vectors containing $N=28\times9=252$ elements.

GLCM is a rotation-dependent technique that performs poorly when textural features change orientation. As explained in the next subsections, we propose to use orientation information derived from the image to constrain that algorithm.

2.3. N-th order circular neighborhood systems

The main problem when deriving GLCM features from image textures stems from the anisotropic sampling of the picture due to the rectangular pixel grid. Our goal was to compute texture features in any direction.

Deng and Clausi explain the principle of the N-th order Circular Neighborhood Systems (CNS). We use a CNS to sample displacement pixels for GLCM. The sampled pixels are all situated on concentric circles of radius r=1, r=2, r=3, … r=O where O is the order of the CNS. For the sake of computational speed, we use bilinear interpolation to interpolate the intensity values of samples that do not fall on the center of pixels (Deng and Clausi, 2004).

Fig. 3(a) below gives an example of a circular 4-th order CNS, with respectively 4, 6, 8, and 10 samples taken on the semi-circles of radius r1=1, r2=2, r3=3, and r4=4, accounting for a total of 4+6+8+10=28 displaced pixels. We chose 28 displacements for the 4-th order CNS, because such a sampling provides a complete coverage of each pixel in the CNS without multiple sampling of the same pixel or pair of pixels. Samples are located on semicircles since GLCMs are symmetric (Materka and Strzelecki, 1998). We chose the 4^{th} order because it was a trade-off between the complexity of the textures that could be thus sampled and computational and storage requirements.

The outcome of the CNS sampling is that there are 28 displacement pixels for each pixel of the image. In our implementation, we generate 28 displacement images.

2.4. Local orientation-controlled Circular Neighborhood System

As mentioned above, we propose a new approach in texture and pattern analysis that relies on a rotation-controlled computation of texture features, using the local orientation field, i.e. two matrices describing the X and Y components of the main local orientation vectors at a given scale. In order to estimate the local orientation field, we retrieve the principal vector of the orientation field over a sliding window of fixed size (that we also call the kernel), using Principal Component Analysis (Randen et al., 2000). Typically, when performing the multi-resolution analysis described in this article, we give the orientation field kernel at least the same size as the reference pattern. In this way, we ensure that the orientation field is at the same scale used for assessing the quasi-stationarity of the image.

Let $\mathbf{u}$ and $\mathbf{v}$ be the coordinate row vectors of the CNS sampling points in the X-Y plane for a rotation angle of 0, and $\mathbf{u}'$ and $\mathbf{v}'$ their result after a rotation of angle φ in the rotation-guided CNS sampling. Therefore,

$$\begin{bmatrix}\mathbf{u}'\\ \mathbf{v}'\end{bmatrix} = \begin{bmatrix}\cos(\varphi) & \sin(\varphi)\\ -\sin(\varphi) & \cos(\varphi)\end{bmatrix}\begin{bmatrix}\mathbf{u}\\ \mathbf{v}\end{bmatrix}. \quad (3)$$

This rotation-guided CNS is illustrated on Fig. 3(b) and is used to derive GLCM textural feature vectors $F_{1,x,y}$ on sliding windows of the image.

2.5. Scale transform of the Circular Neighborhood System

An important component of the multi-scale analysis scheme described in this article is the scale transformation of the reference pattern using dilations along the *X* or *Y*-axis. The multi-scale analysis is achieved not only by having multi-scale textural features from GLCM, but also by measuring a similarity distance between textural features computed on samples of the image and textural features computed on dilated versions of the reference pattern.

In order to capture textural features at a given scale and orientation, we apply scale transforms to rotation-guided CNS. Our approach is the reverse of the stochastic generation of images through MPGS, where local scale and orientation information can be used to control the realization of a stochastic process and enables the repetition of a pattern at varying scales and orientations (Caers, 2003). Metzler et al. (1995) propose a method based on cross-scale co-occurrence matrices to classify images in the scale space. Our approach also differs from Metzler's, because we work in a 2-D scale space with different *X*/*Y* aspect ratios, and we explicitly integrate the orientation constraint in GLCM.

The scale factors a_x and a_y describe the scale transform of the reference pattern. An angle-preserving scale change without distortion of the patterns or textures corresponds to $a_y=a_x$. We apply the scale transforms to CNS coordinates before rotating them and the total scale and rotation transformation of the CNS is

$$\begin{bmatrix} \mathbf{u}'' \\ \mathbf{v}'' \end{bmatrix} = \begin{bmatrix} a_x & 0 \\ 0 & a_y \end{bmatrix} \begin{bmatrix} \cos(\varphi) & \sin(\varphi) \\ -\sin(\varphi) & \cos(\varphi) \end{bmatrix} \begin{bmatrix} \mathbf{u} \\ \mathbf{v} \end{bmatrix}. \quad (4)$$

Fig. 3(c) illustrates a rotated and scaled CNS. Fig. 4 shows an image with a superimposed orientation field and, at various locations on the image, examples of local orientation-constrained CNS with different scales. Orientation-and-scale-constrained CNS is used to derive GLCM textural feature vectors $F_{0,sx,sy}$ on the reference pattern.

3. Applications

3.1. Derivation of the scale field of an image

Once the image is decomposed by a multi-scale pattern matching analysis, a scale map showing distances between $F_{0,sx,sy}$ and $F_{1,x,y}$ can be displayed. We note this map $\{S_{i,j}\}$, where $i \in \{1, N_x\}$, $j \in \{1, N_x\}$. For a given dilation number *i* along the *X*-axis and dilation number *j* along the *Y*-axis, $S_{i,j}$ shows the Euclidian distance between small zones of the image and the dilated reference pattern. The bigger the size *D* of the sampling window (and of the reference pattern), the more textural data are captured within that window. For speed issues, we do not perform the multi-scale matching analysis on a pixel-by-pixel basis but sample the image every τ pixels. Reducing τ yields a more precise map. Another possible display is a scale-space image that highlights only the best match for each small zone of the image. Fig. 5 shows two example images, with their orientation fields, scale distance maps and scale-space images.

3.2. Scale stationarity of images

Under the assumption of quasi-stationarity, we measure scale stationarity, relative to a reference pattern, by the departure from a single clustered value of **a**=(1,1) on the scale-space image . Hence any variation along the *X* or *Y*-axis of the scale-space image indicates a non-stationary image.

In order to measure the scale stationarity of the image, we provide a measure of the spread of the cloud of points $p_1, p_2, \ldots p_n$ defined by the best matches between the image and the dilated patterns, each point corresponding to a unique zone on the image. $p_1, p_2, \ldots p_n$ are associated coordinates $x_1, x_2, \ldots x_n$ and $y_1, y_2, \ldots y_n$ on the scale-space image by uniquely mapping dilation factors to abscissas (for instance $\{1/2,\ 2/3,\ 3/4,\ 1,\ 4/3,\ 3/2,\ 2\}$

respectively correspond to $\{-1,\ -2/3,\ -1/3,\ 0,\ 1/3,\ 2/3,\ 1\}$, as illustrated on Fig. 6). Thanks to Singular Value Decomposition we get the two principal components and singular values σ_1 and σ_2 of $p_1, p_2, \ldots p_n$. The first principal component gives the direction of the strongest variation of $p_1, p_2, \ldots p_n$, and the ratio σ_2/σ_1 informs us about the aspect-ratio variability. Using SVD notation (Krzanowski, 1998), we write

$$(5) \qquad \begin{bmatrix} x_i \\ y_i \end{bmatrix}_{i\in[1,n]} = \mathbf{USV}^T \quad \text{and} \quad \begin{bmatrix} u_i \\ v_i \end{bmatrix}_{i\in[1,n]} = \mathbf{U} \times \begin{bmatrix} x_i \\ y_i \end{bmatrix}_{i\in[1,n]},$$

and define the scale stationarity factor

$$(6) \qquad S = \max\left\{0,\ 1 - \mathrm{var}(u_i)_{i\in[1,n]}\left(\frac{\sigma_1+\sigma_2}{\sigma_1}\right)\right\}.$$

A scale stationarity score of S=100% occurs when all the scales are (1,1).

The scale stationarity score can be considerably influenced by the initial choice of the reference pattern (location and size), although we verify on one example in Section 4 that small changes in the location of the reference pattern (a few pixels) do not affect the scale-space images considerably. Therefore we propose to estimate the scale stationarity score by subdividing the image into 9 overlapping zones $Z_1, Z_2, \ldots Z_9$ (see Fig. 2), consecutively using each of those zones as the reference pattern and averaging the scale stationarity scores.

4. Results and discussion

4.1. Scale estimation on synthetic chirp images

The first series of tests were aimed at testing whether our algorithm is able to accurately estimate scale-factor variations on an image where the scale changes are known. They also attempted to ascertain whether the method is stable with regards to the choice of different parameters: numbers of scales N_x and N_y, size of the sliding window D, scale-space image sampling step τ, location of the reference pattern, whether the aspect ratio is equal to 1 or not, and whether the orientation field is used to constrain the CNS or not.

For this purpose we generated "spatial chirp" images. . In signal processing, a chirp signal is a sinusoidal wave whose frequency increases or decreases with time or distance, e.g. linearly, according to $g(t) = A(t)\cos(\alpha t^2)$. By extrapolation to 2D, chirp textures are purely synthetic images that display an elementary texture consisting in a spatial alternation of black and white lines (or patches) with an additional continuous variation of spatial frequency. Chirp texture images have been used as a simplistic model of woodgrain or fingerprint images, in order to test frequency analysis algorithms (Pattichis and Bovik, 2007), or to model a pattern with continuously changing scale for texture segmentation algorithms (Sagiv et al., 2006).

Chirp texture images can be perfectly characterized in terms of scale and orientation using spectral methods. We combined (either add or multiply) a frequency chirp along the X-axis $\cos(f(x)x)$ with another one along the Y-axis $\cos(f(y)y)$ in order to independently change the X and Y frequency on the image (see Fig. 7, where x and y vary from 0 to 51.1 by increments of 0.1, the values of f vary from 1/3 to 3 by increments of (3-1/3)/512 and all images are 512x512 pixels).

We proceeded in a similar way to generate a 512x512 pixels radial equivalent of a chirp image illustrated on Fig. 7, following the equation $\cos(k_1 \times \mathrm{angle}(x+iy))$ where k_1=50, x and y are between [-25.6, 25.5] and are incremented by 0.1.

On the horizontal/vertical chirp images, we estimated the change of scale using local frequencies $f(x)$ and $f(y)$ at any given pixel (x,y) and relative to frequencies $f(x_0)$ and $f(y_0)$ in the middle of the reference pattern selected at the center of the image. This yielded $s(x) = f(x_0)/f(x)$ and $s(y) = f(y_0)/f(y)$. $s(x)$ ranges from 1/3 to 3 from left to right, and $s(y)$ likewise ranges from 1/3 to 3 from bottom to top. We computed corresponding theoretical scale-space

images $\{S'_{i,j}\}$ using the same scale factors, same location of reference pattern and same values of D and τ as on estimated scale-space images $\{S_{i,j}\}$.

We measured the accuracy of our method and assessed the impact of each of its parameters, by comparing $S_{i,j}$ and $S'_{i,j}$. We established two classification scores: a "hard" score that considers that a scale assigned to a wrong bin (for instance ×3/2 instead of ×2) is misclassified, and a "soft" score that allows an error of 1 bin in classification (×3/2 instead of ×2 will not be considered as a misclassification, but ×4/3 instead of ×2 will).

First we performed tests on the horizontal/vertical chirp images ignoring the orientation field. Table I shows results both for testing at different locations of the reference pattern around the center of the image, using different values of D and τ, and two different image resolutions, resulting with hard classification scores over 60% and a soft classification scores between 93% and 100%. Fig. 8 shows that visually there is a very small difference between scale-space images yielding the highest classification score (1) and the lowest classification score (2). Table II shows results for testing with different sets of discrete scale transforms. Although the soft and hard classification scores are relatively low for the parameters set (3), this may be due to the large number of scale factors that make it more probable to misclassify an area of the image by two scale factors or more. Chirp_2 obtained classification rates of 99.3% (soft) and 73.6% (hard), Chirp_3 obtained 100% (soft) and 71.6% (hard), and Chirp_4 obtained 94.4% (soft) and 61.8% (hard). All rates were obtained with the same set of parameters as in (1).

The next test performed on Chirp_1 (see Fig. 7) was aimed at measuring the influence of the orientation field constraint, on scale classification results. Fig. 9 shows that the orientation field of the image is symmetric relative to the diagonal of the image, horizontal on the upper left part of the image, and vertical on the lower right because the orientation field follows the elongation of features. When taking into account that symmetry for the theoretical scale-space image, the method achieves good soft and hard classification rates (98.6% and 56.9% respectively).

We performed a series of tests to assess the relative importance and the discriminant power of different GLCM textural features, by either removing GLCM textural features one by one or by keeping only one of them. The orientation field is not used as a constraint here. Table III shows that two textural features, energy and maximum probability give bad scale classification results if used alone, and that removing both of them and keeping the remaining 7 textural features still yields good soft and hard classification results, respectively 100% and 67.3%. These tests are however specific to Chirp_1.

The last series of tests were performed on a radial chirp image (Fig. 10) using a constant aspect ratio of 1. We estimated the local scale factor using the length of the arc linking two adjacent black radii originating from the center of the image, i.e. $2\tan(2\pi/k_1)\sqrt{x^2+y^2}$. The classification results obtained when the GLCM texture features are constrained by the local orientation field are much better (96.6% soft and 78.1% hard classification) than without it (45% and 29%).

4.2. Scale and scale stationarity estimation on the Brodatz natural textures database

We extended our study to natural textures and tested our scale estimation method on the Brodatz textures database, initially consisting of 112 photographic images. Most of those images can be considered as quasi-stationary because they correspond to a pattern repeated several times over the image. First, we computed scale stationarity scores and corresponding scale-space images using seven scale factors $\{1/2,\ 2/3,\ 3/4,\ 1,\ 4/3,\ 3/2,\ 2\}$, nine reference patterns arranged as on Fig. 2, and variable sizes of the orientation kernel. All images were 214x214 pixels, except for D6 which was 320x320. The reference patterns had a size of 108x108 with a sampling of 27x27 (160x160 with a sampling of 40x40 for D6). In order to ensure that we were working on quasi-stationary images, we selected a subset of 48 images that obtain a scale stationarity score of 100% for at least one among the 9 reference patterns (see Table IV).

In a second step, we generated composite images as illustrated on Fig. 11, where the four quarters have scales (1, 1), (1, 1/2), (1/2, 1) and (1/2, 1/2). We then ran the scale classification using 4 scale factors $\{1/2,\ 2/3,\ 3/4,\ 1\}$ and chose as reference pattern the quarter of image that has a scale (1, 1). We collected the number of correct scale estimations using the following scoring scheme: for each of the other three corners of the image, a correct prediction contributed 1 unit, an error of one scale factor (e.g. 2/3 instead of ½ along the X or Y axis) contributed 0.5, an error

of two scale factors (e.g. 3/4 instead of 1/2) contributed 0.25. Otherwise the contribution was set to 0. The maximum possible scale estimation score per image is 3. Table IV summarizes our results. The average scale estimation score is 1.9 (which is equivalent to having two correct scale predictions and the remaining one incorrect or one correct scale prediction and the remaining two with a small estimation error). 64% of (1, 1/2) and (1/2, 1) scales, and 62% of (1/2, 1/2) scales were correctly estimated.

On our image data set, we propose five possible explanations for scores lower than 2:

(a) Six images have a non-stationary orientation field. Therefore, there is no link between the scale transform applied to the rectangular image and the scale transforms applied to the rotation-controlled stencil of our textural feature descriptor (and our test is not appropriate for that kind of image).

(b) Three images have a diagonal orientation field that gets distorted when we apply (1, 1/2) and (1/2, 1) scale transforms. Our algorithm was indeed designed for detecting scale changes applied before a rotation. A possible extension would be to test for scale changes following a rotation.

(c) On seven images, the orientation field changes after applying scale transforms. As in b), this is because our algorithm was designed for detecting scale changes applied before rotation.

(d) One image is nearly invariant along the Y direction.

(e) Sampling artifacts appear on four images after applying scale transforms (due to poor image resolution and high level of texture details), thereby affecting extraction of the rotation field. A better noise-proof algorithm for orientation field extraction could help alleviate this problem.

4.3. Scale stationarity estimation on a bank of training images for Multipoint Geostatistics

In the introduction, we indicated that one motivation of our research was the stationarity requirement of training images for MPGS, a technique often used in Earth Sciences (Caers 2003). The majority of the training images used in our study represent geological bodies like river channels or sedimentation models.

We ran our algorithm on a bank of 31 images. The size of the kernel used for the computation of orientation and the extraction of GLCM textural features is ½ of the image length or width (whichever is smaller). The textural features were sampled every ¼ of the kernel size. We computed nine GLCM textural features on 32-gray-level images. Seven scales factors $\{1/2,\ 2/3,\ 3/4,\ 1,\ 4/3,\ 3/2,\ 2\}$ were used. Fig.12 shows the training image database and scale stationarity classification results, which seem to give a plausible interpretation of the image scale stationarity. The only major exception is the second image from the right in the second row from the top, to which the method attributed a score of 95% although visual appraisal might indicate a lower score.

A further study showed that there was a very good correlation between the combined scale and orientation scores and the quality of the outcome of a training image when used with the current MPGS stochastic image generation algorithms. Our method is consequently able to estimate image scale stationarity for the application of MPGS.

5. Conclusions

In this article we showed that our method manages to correctly estimate scale variations on quasi-stationary images such as textured images and geological training images for MPGS. Moreover, we have introduced a new approach to multi-scale texture analysis, which diverges from the mainstream approach of obtaining rotation-invariant texture descriptors, and instead strives at integrating rotation information in order to constrain the texture descriptors. A possible extension of this study would be to compare the discriminative power and classification performances of orientation-constrained GLCM versus rotation invariant texture descriptors.

6. Acknowledgments

P. W. Mirowski and D. Tetzlaff thank the Geology and Rock Physics Department of Schlumberger-Doll Research, namely Claude Signer, David McCormick, and Nneka Williams, as well as Roy Davies from Rocksource, for their

valuable contributions and advice in matters of geology and for testing the scale stationarity on geological images for the application of Multipoint Geostatistics. They also thank Michael Prange and Nicholas Bennett from Schlumberger-Doll Research, Ashley Wieringa from Schlumberger Information Solutions, and four anonymous reviewers for helpful advice on improving this article.

References

Arivazhagan, S., Ganesan, L., Padam Primal, S., 2006. Texture classification using Gabor wavelets based rotation invariant features. Pattern Recognition Letters, vol. 27, no. 16, pp. 1976-1982.

Pattichis, M.S., Bovik, A.C., 2007. Analyzing Image Structure by Multidimensional Frequency Modulation. IEEE Transactions on Pattern Analysis and Machine Intelligence, vol. 29, no. 5, pp. 753-766.

Bradley, A., Jackway, P., Lovell B., 1995. Classification in scale-space: applications to texture analysis. Proceedings of the International Conference on Information Processing in Medical Imaging 1995, pp. 375-376.

Brodatz, P., 1966. Textures: A photographic Album for Artists and Designers. Dover, New York. Available online at: http://www.ux.his.no/~tranden/brodatz.html.

Caers, J., 2003. History matching under training-image based geological model constraints. Society of Petroleum Engineers Journal 2003, pp. 218-226.

Caers, J., Zhang, T., 2004. Multiple-point geostatistics: a quantitative vehicle for integration of geologic analogs into multiple reservoir models, in: Grammer, M., Harris, P.H., Eberli, G.P., (Eds.), Integration of Outcrop and Modern Analogs in Reservoir Modeling. Tulsa, OK, AAPG Memoir 80.

Clausi, D., Zhao, Y., 2002. Rapid extraction of image texture by co-occurrence using a hybrid data structure. Computers and Geosciences, vol. 28, no. 6, pp. 763-774.

Deng, H., Clausi, D., 2004. Gaussian MRF Rotation-Invariant Features for Image Classification. IEEE Transactions on Pattern Analysis and Machine Intelligence, vol. 26, no. 7.

Haralick, R.M., Shanmugham, K.S., Dinstein, I., 1973. Texture Features for Image Classification. IEEE Transactions on Systems Man and Cybernetics, SMC-3, no. 6, pp. 610-621.

Huang, K., Aviyente, S., 2006. Rotation Invariant Texture Classification with Ridgelet Transform and Fourier Transform. Proceedings of the IEEE International Conference on Image Processing 2006, pp. 2141-2144.

Krzanowski, W.J., 1988. Principles of Multivariate Analysis: A User's Perspective. Oxford Statistical Science Series, vol.3. Oxford University Press, Oxford.

Mallat, S.G., 1999. A wavelet tour of signal processing. Second edition, Academic Press.

Manjunath, B.S., Ma, W.Y., 1996. Texture Features for Browsing and Retrieval of Image Data. IEEE Transactions on Pattern Analysis and Machine Intelligence, vol. 18, no. 8.

Manjunath, B.S., Ma, W.Y., 1996. Texture Features and Learning Similarity. Proceedings of the IEEE Computer Society Conference on Computer Vision and Pattern Recognition 1996, pp. 425-430.

Manthalkar, R., Biswas, P.K., Chatterji, B.N., 2003. Rotation and scale invariant texture features using discrete wavelet packet transform. Pattern Recognition Letters, vol. 24, pp. 2455-2462.

Materka, A., Strzelecki, M., 1998. Texture Analysis Methods – A Review. Technical University of Lodz, Institute of Electronics, COST B11 report, Brussels.

Metzler, V., Palm, C., Lehmann, T., Aach, T., 2000. Texture Classification of Gray Level Images by Multiscale Crossco-Occurrence Matrices. Proceedings of the IEEE International Conference on Pattern Recognition ICPR 2000, vol. 2, pp. 549-552.

Ojala, T., Pietikäinen, M., Mäenpää, T., 2002. Multiresolution Gray-Scale and Rotation Invariant Texture Classification with Local Binary Patterns. IEEE Transactions on Pattern Analysis and Machine Intelligence, vol. 24, no. 7, pp.971-987.

Randen, T., Husoy, G., 1999. Filtering for Texture Classification: a Comparative Study. IEEE Transactions on Pattern Analysis and Machine Intelligence, vol. 21, no. 4, pp.291-310.

Randen, T., Monsen, E., Signer, C., Abrahamsen, A., Hansen, J.O., Sater, T., Schlaf, J., Sonneland, L., 2000. Three-Dimensional Texture Attributes for Seismic Data Analysis. Society of Exploration Geophysicists Technical Program Expanded Abstracts 2000, pp. 668-671.

Sagiv, C., Sochen, N.A., Zeevi, Y.Y., 2006. Integrated Active Contours for Texture Segmentation. IEEE Transactions on Image Processing, vol. 15, no. 6, pp. 1633-1646.

Tetzlaff, D., Davies, R., McCormick, D., Signer, C., Mirowski, P., Williams, N., 2005. Application of multipoint geostatistics to honor multiple attribute constraints applied to a deepwater outcrop analog, Tanqua Karoo Basin, South Africa. Society of Exploration Geophysicists Technical Program Expanded Abstracts 2005, pp. 1370-1373.

Visa, A., 1990. Identification of Stochastic Textures with Multi-resolution Features and Self Organizing Maps. Proceedings of the IEEE International Conference on Pattern Recognition ICPR 1990, vol. 1, pp. 518-522.

Zhang, D., Wong, A., Indrawan, M., Lu G., 2000. Content-Based Image Retrieval Using Gabor Texture Features. Proceedings of the First IEEE Pacific-Rim Conference on Multimedia 2000, pp. 1139-1142.

Figure captions

Fig. 1 Nine overlapping zones used to decompose an image.

Fig. 2 Full description of the method for retrieving scale maps and scale stationarity statistics from images using the orientation information.

Fig. 3 Example of a fourth-order CNS. (a) has a rotation of theta = 0 and scale factors (1,1), (b) a rotation of theta = -60deg and scale factors (1,1), and (c) a rotation of theta = -60deg and scale factors (½,1). An scale factor of ½ for the X-axis means that the CNS sampling "zooms" along the X-axis when sampling the pattern. It is equivalent of dilating the pattern by a factor of 2 along the X-axis.

Fig. 4 Example of an image with a superimposed orientation field and fourth-order circular neighborhood systems that have undergone rotation transforms according to the local orientation field. ***a***, ***b***, ***c*** all have scale factors of (1, 1), and the other neighborhood systems have the following scale factors: ***d*** (2,2), ***e*** (2,3/2), ***f*** (2,½), ***g*** (3/4,2), ***h*** (3/2,4/3), ***i*** (1,¾), and ***j*** (½,½).

Fig. 5 (a) Synthetic 256×256 pixels image with a 64×64 pixels reference pattern delimitated by a rectangle, (b) corresponding orientation field computed on kernels of size 64×64 pixels sampled every 16 pixels, (c) scale distance map sampled every 16 pixels derived from the image, and (d) subsequent scale-space image . The reference pattern appears on the middle (1, 1) image of (d). (e) 287×191 pixels picture of a weaved basket with a 32×32 pixels reference pattern (on the left), (f) corresponding orientation computed using kernels of size 64×64 pixels sampled every 16 pixels, (g) scale distance map and (h) scale-space image computed using 3 scale factors per direction $\left\{\frac{3}{4}, 1, \frac{4}{3}\right\}$ and sampled every 8 pixels.

Fig. 6 Example of a scale-space representation of the "spread" of an image across different scales, with superimposed first and second principal component of the cloud of points.

Fig. 7 Horizontal/vertical chirp images used in the testing of our method.

Fig. 8 Scale-space images (a) and (b) are obtained for Chirp_1 using the set of parameters (1), and scale-space images (c) and (d) using the set of parameters (2). Scale-space images (b) and (d) are theoretical and scale-space images (a) and (c) are the results of our method.

Fig. 9 (a) Estimated and (b) theoretical scale-space images for Chirp_1 using the orientation field constraint (c).

Fig. 10 (a) Radial chirp image, (b) its orientation field and (c) theoretical scale-space image , as well as the scale-space images computed with (d) and without (e) the orientation field constraint. Classification scores are respectively 96.6% (soft), 78.1% (hard) for (d) and 45% (soft), 29% (hard) for (e).

Fig. 11 (a) Brodatz textured image D35, (b) composite image with 4 scale transforms (the orientation field is vertical and stationary over all the image), (c) scale-space image found using 4 scale factors $\left\{\frac{1}{2}, \frac{2}{3}, \frac{3}{4}, 1\right\}$ per dimension and using as a reference pattern the top left quarter of the image with scale (1,1).

Fig. 12 Bank of training images used for Multipoint Geostatistical algorithms simulations, ranked by decreasing scale stationarity score. Images are hand-drawn or taken from (Caers, 2003).

Figure 1

Click here to download high resolution image

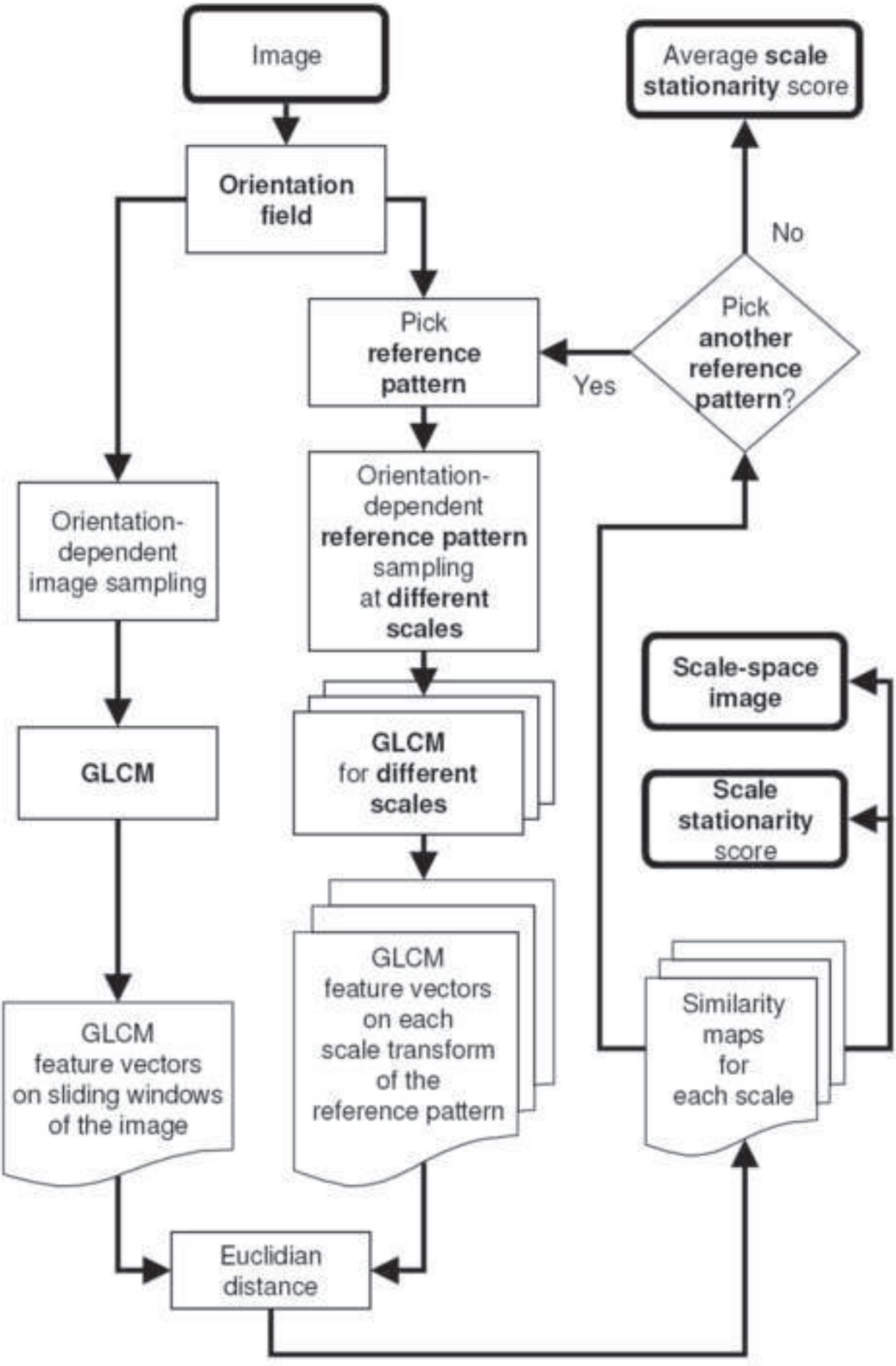

Figure 2

Click here to download high resolution image

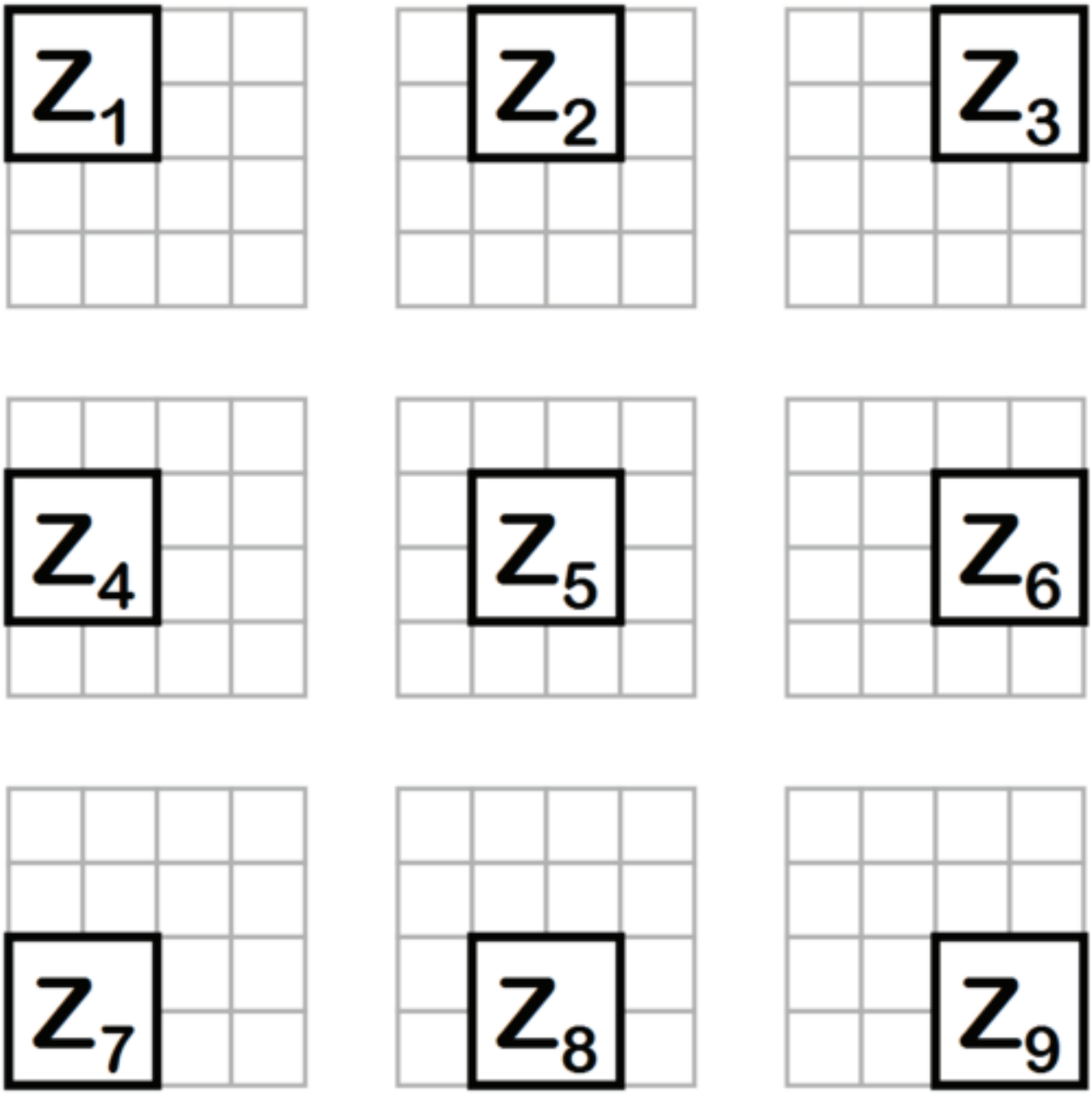

Figure 3

Click here to download high resolution image

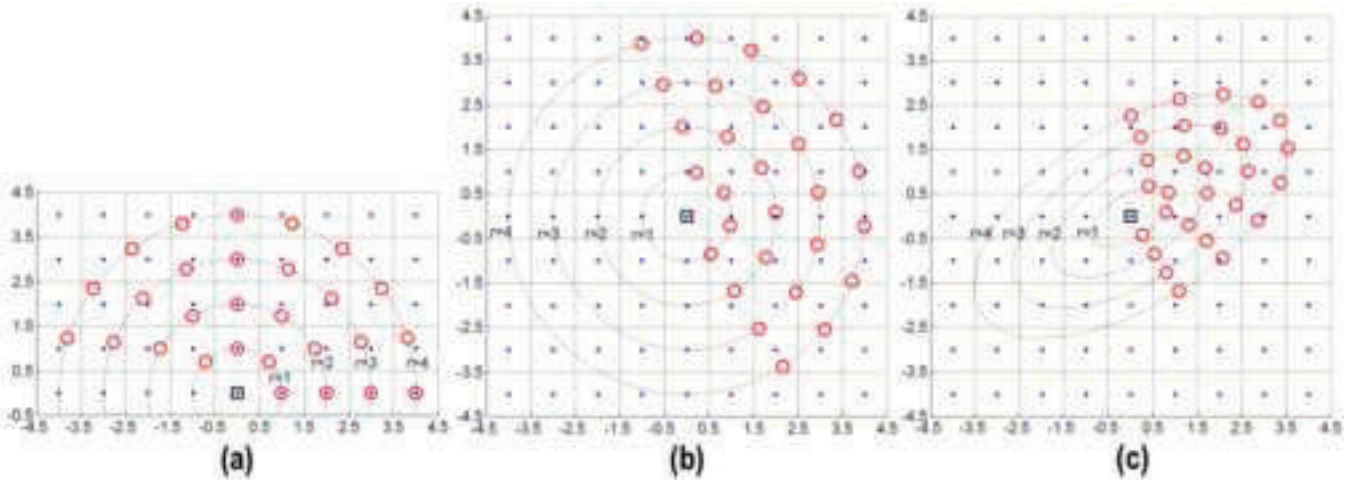

Figure 4

Click here to download high resolution image

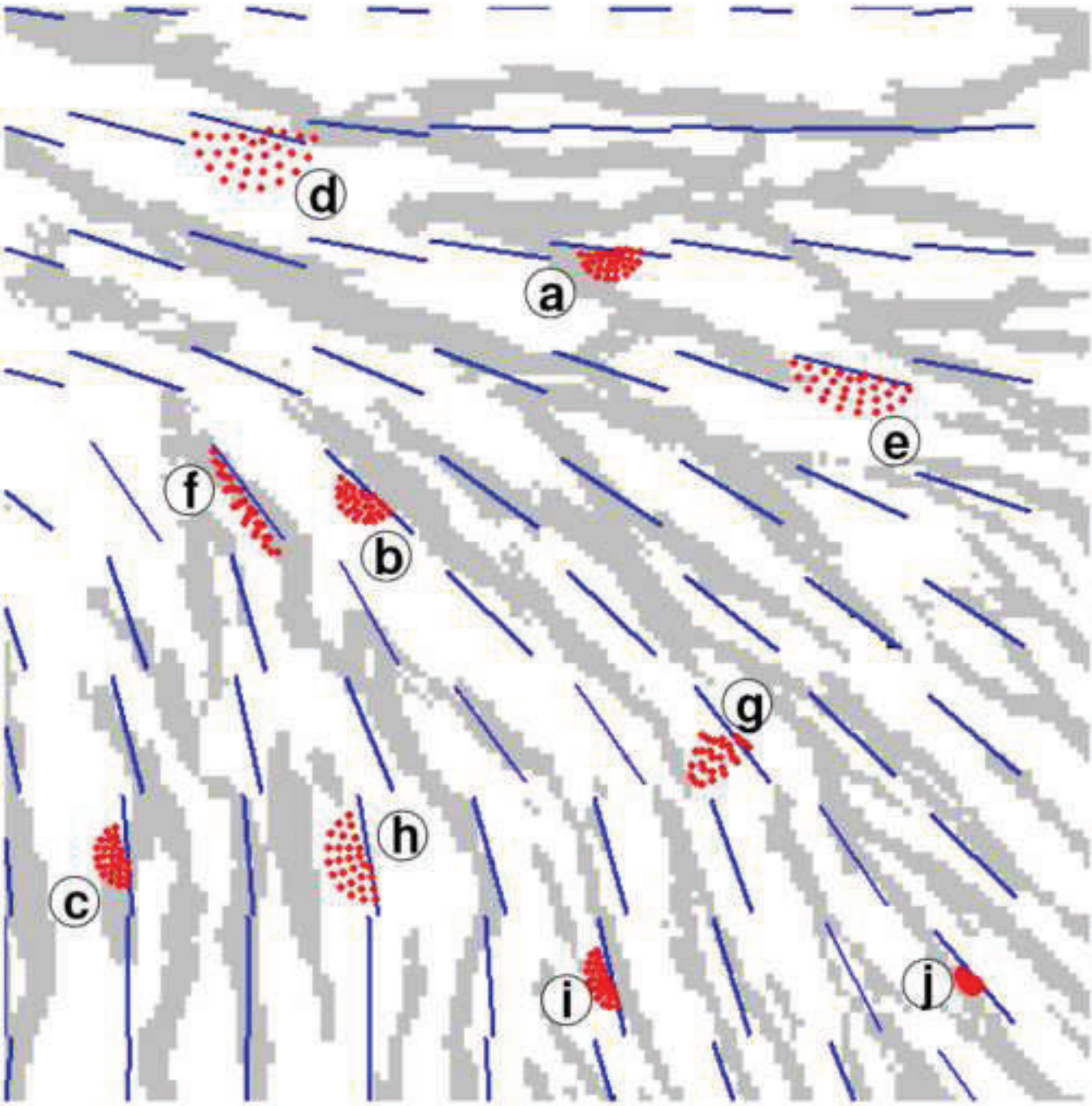

Figure 5

Click here to download high resolution image

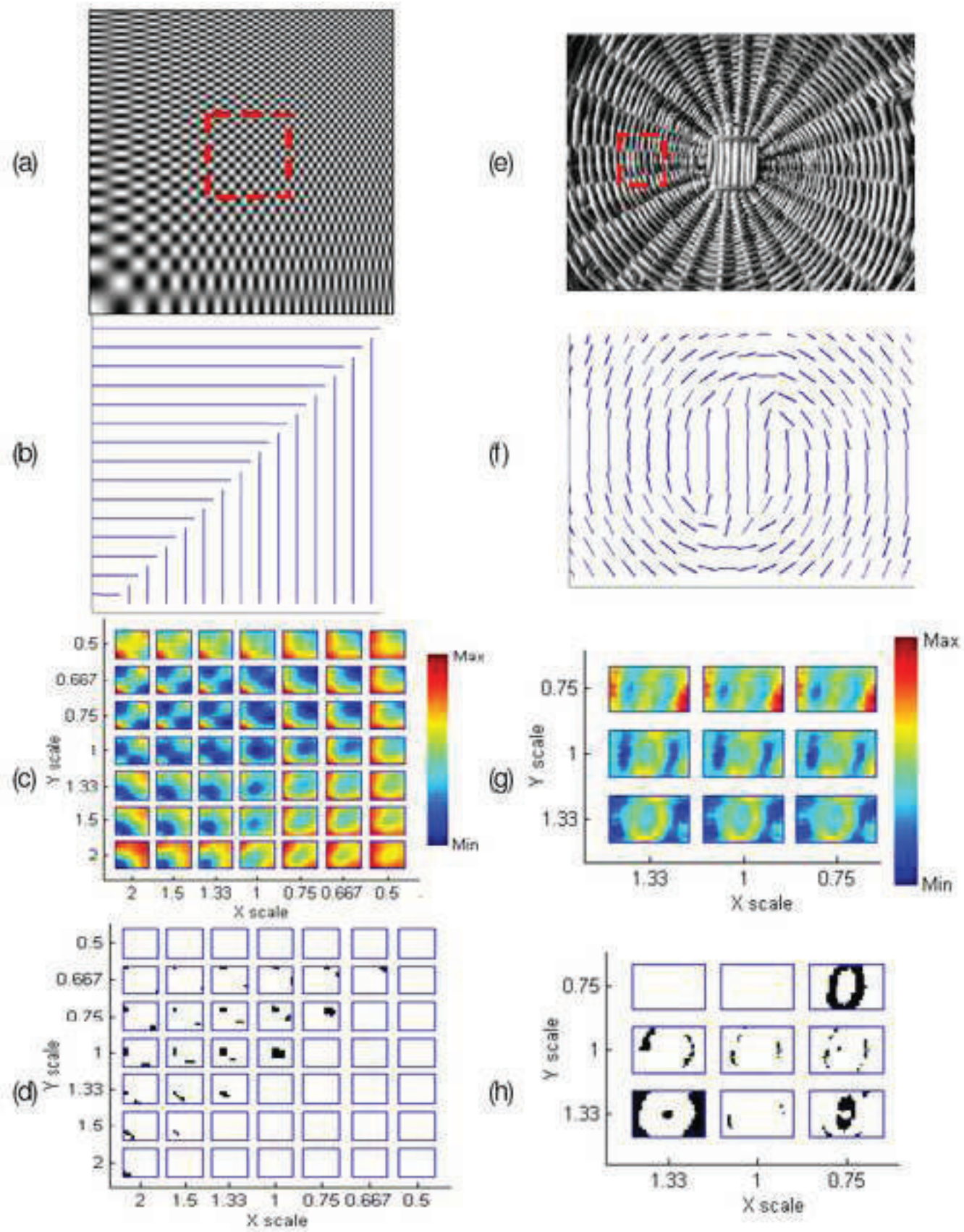

Figure 6
Click here to download high resolution image

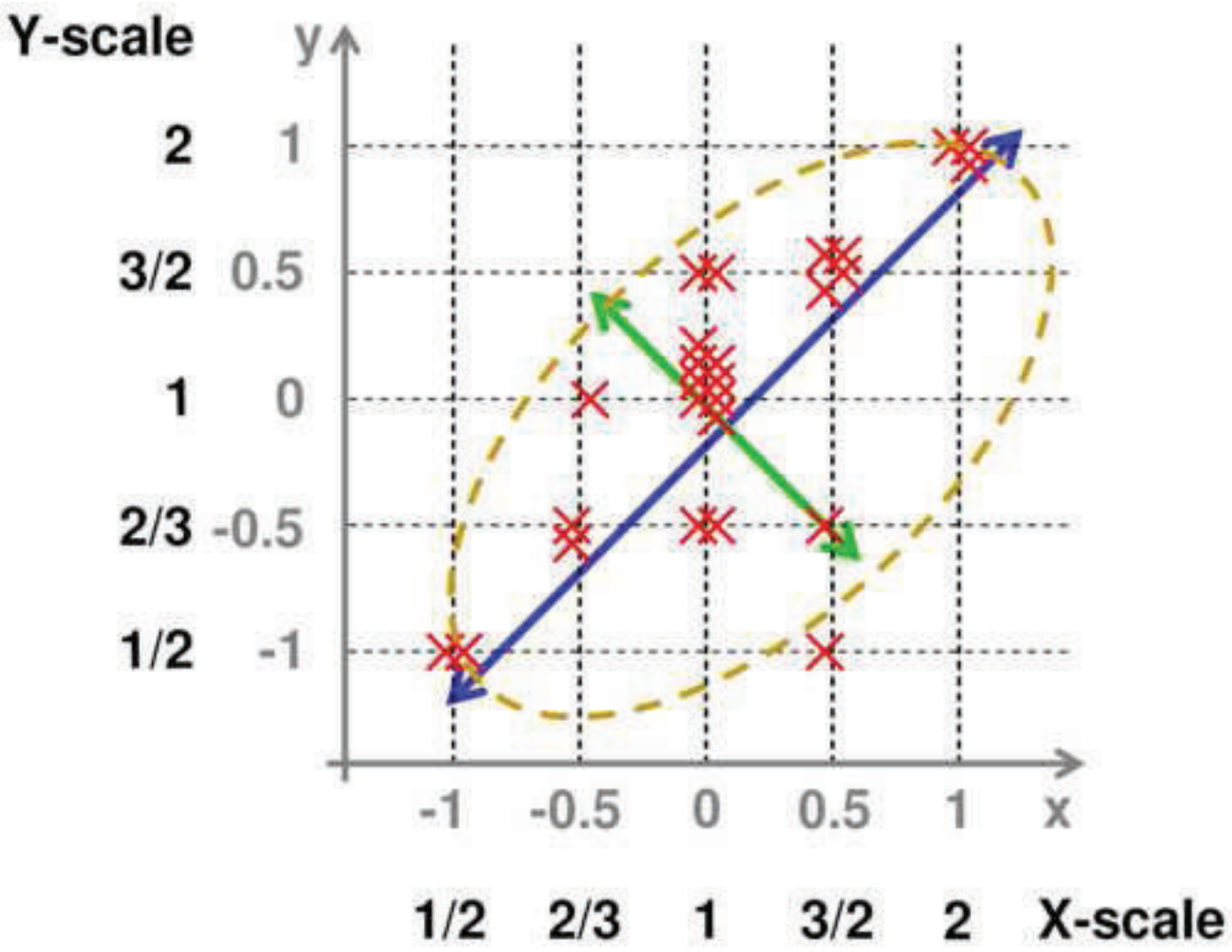

Figure 7

Click here to download high resolution image

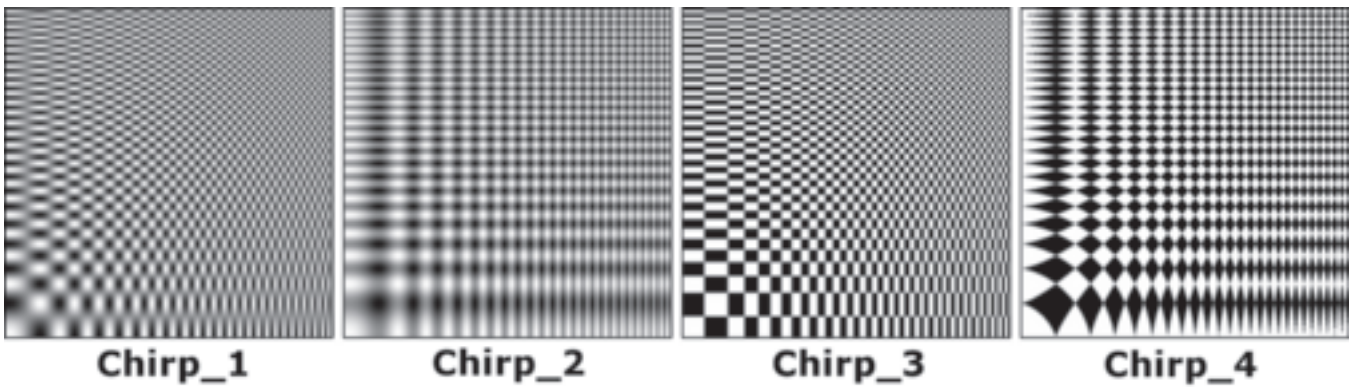

Figure 8

Click here to download high resolution image

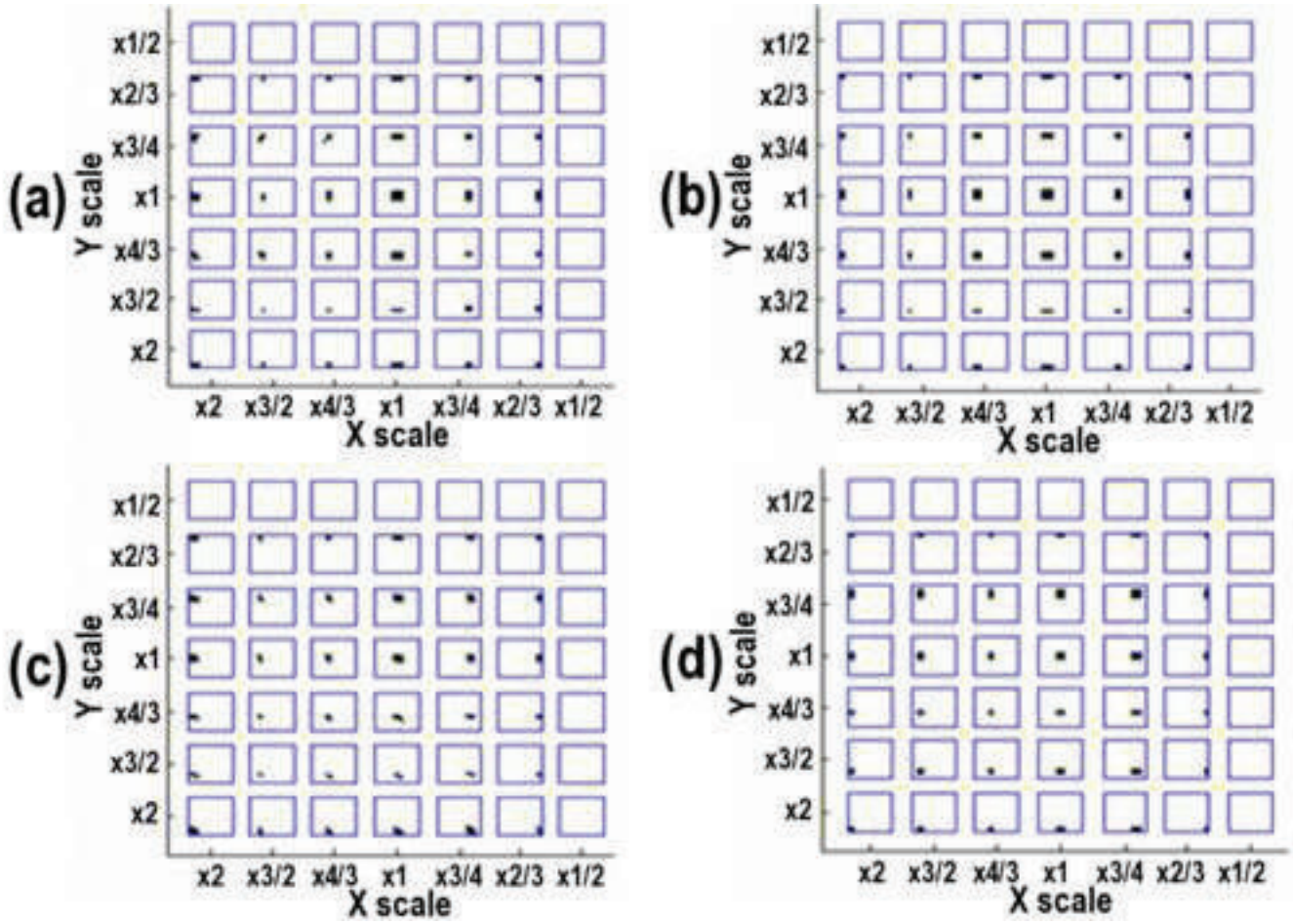

Figure 9

Click here to download high resolution image

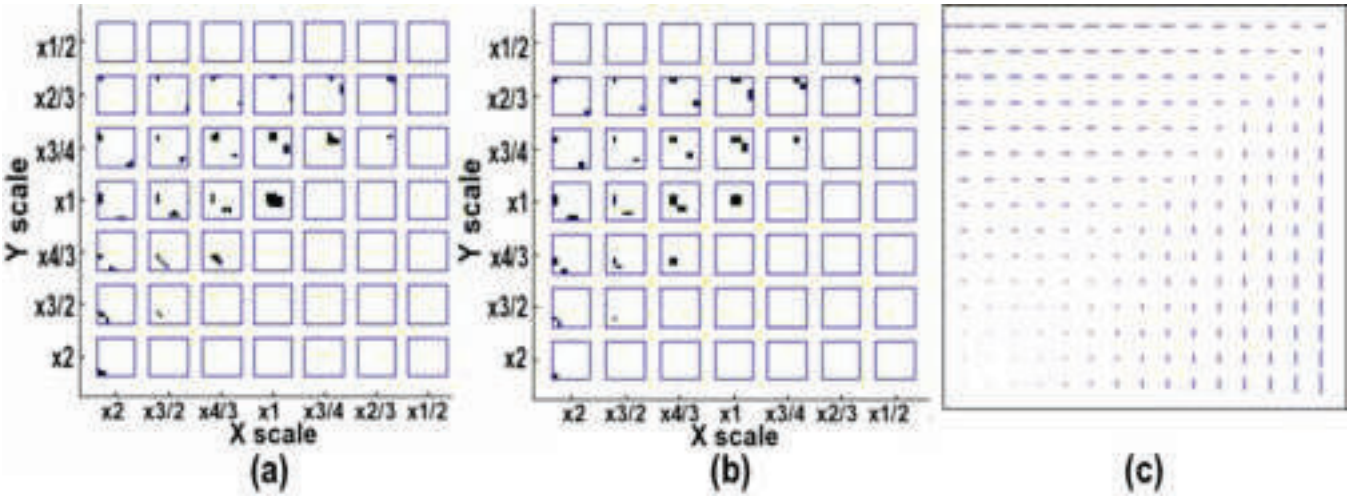

Figure 10

Click here to download high resolution image

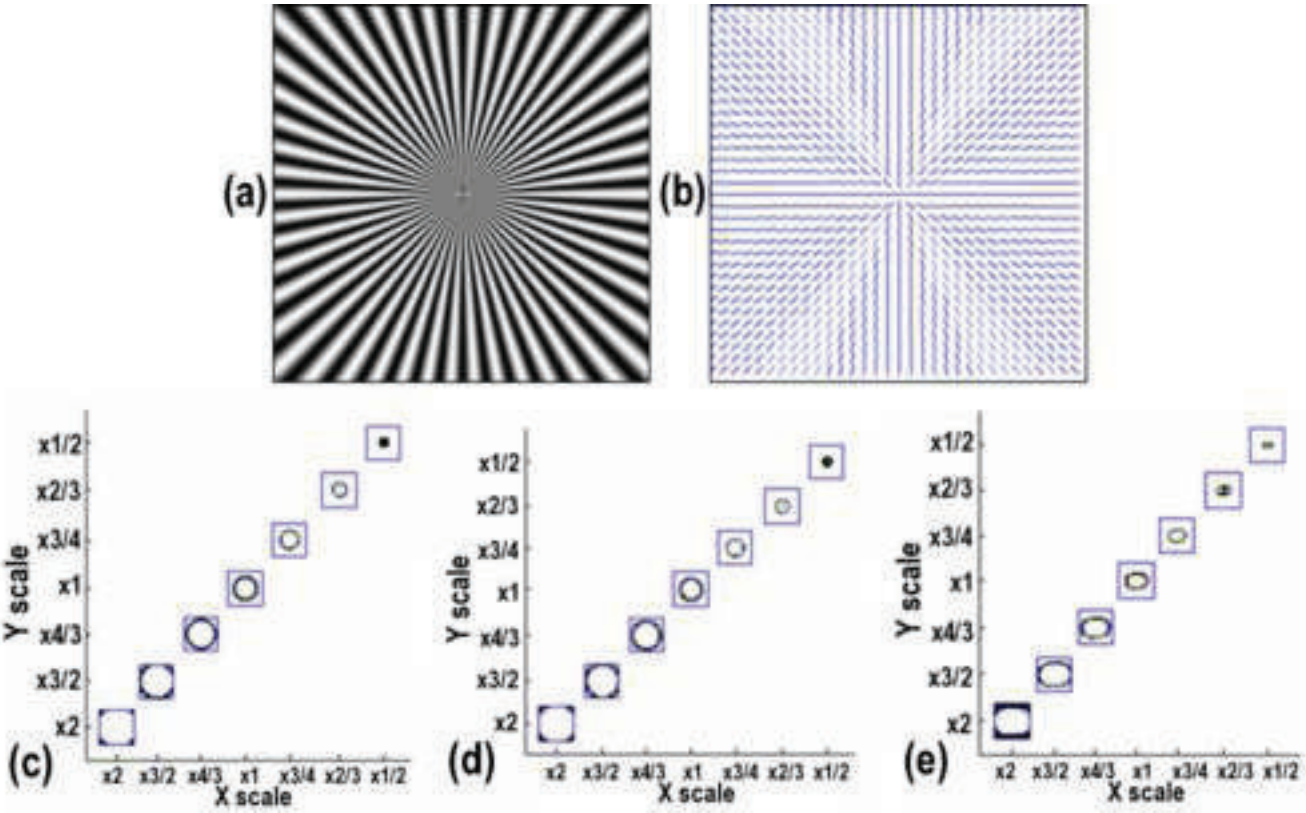

Figure 11

Click here to download high resolution image

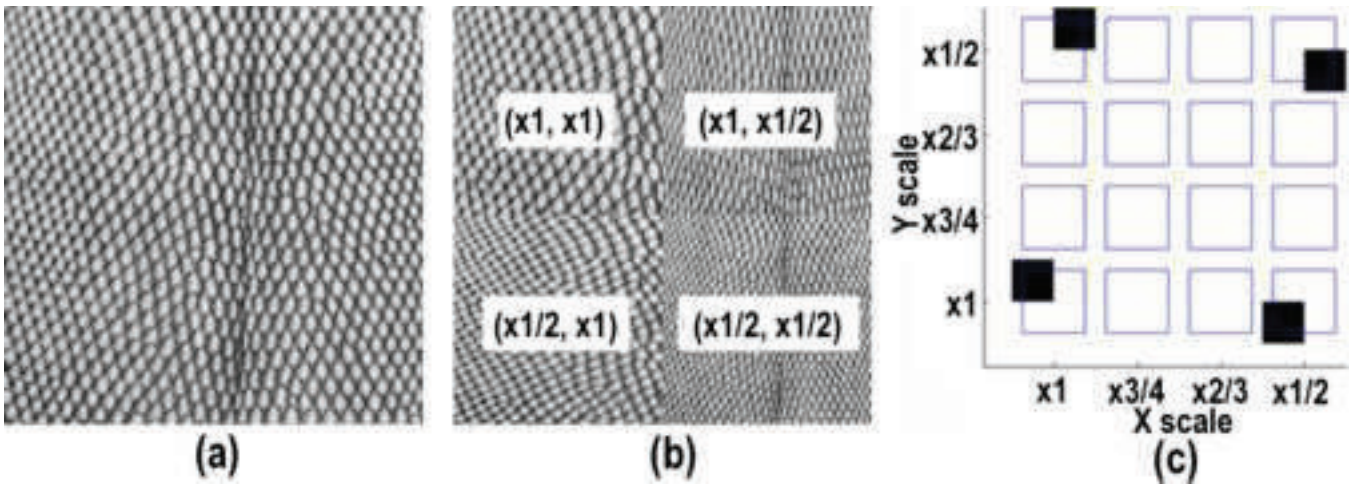

Figure 12

Click here to download high resolution image

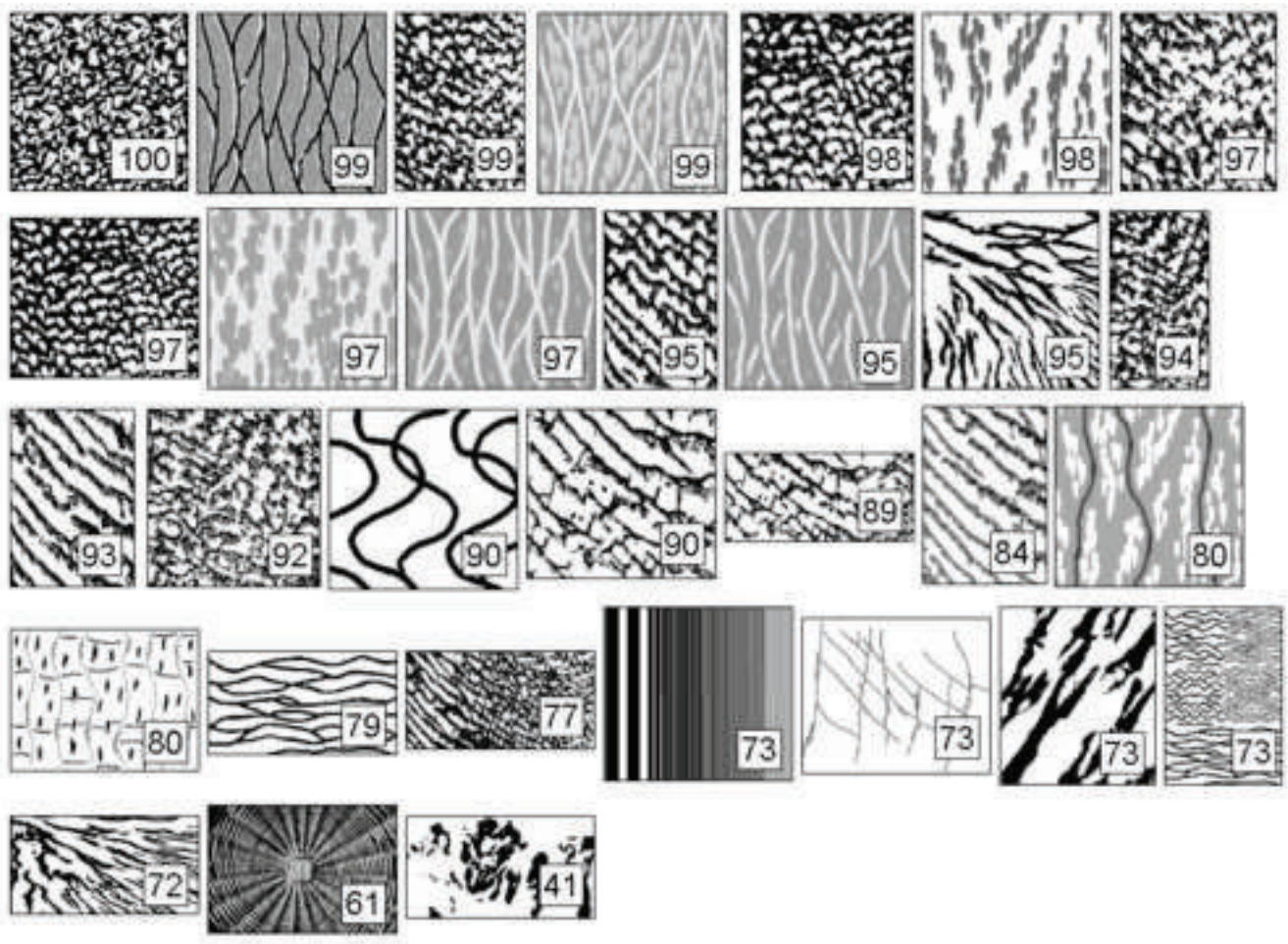

	Image size	*win_size*	*win_step*	Location	Classification score	
					Soft	Hard
	256x256	64	16	(99, 95) to (162, 158)	100.0%	67.4%
	256x256	64	16	(106, 93) to (169, 156)	97.9%	62.5%
(1)	256x256	64	16	(99, 88) to (162, 151)	100.0%	80.6%
	256x256	64	16	(106, 94) to (169, 157)	94.4%	57.0%
	256x256	64	16	(100, 88) to (163, 151)	100.0%	66.0%
	256x256	64	16	(97, 79) to (176, 158)	100.0%	77.1%
	512x512	64	16	(232, 216) to (295, 279)	94.6%	74.1%
	512x512	128	32	(198, 187) to (325, 314)	100.0%	63.9%
(2)	512x512	128	16	(190, 182) to (333, 325)	93.4%	73.3%

Table I: Scale classification scores for Chirp_1 using different locations of the reference pattern around the center of the image, different values of D and τ, and two different image sizes.

	Scales	Classification	
		Soft	Hard
	x0.5 x0.75 x1 x1.33333 x2	100.0%	81.3%
	x0.5 x0.66667 x1 x1.5 x2	100.0%	83.3%
	x0.5 x1 x2	99.3%	72.9%
	x0.5 x0.66667 x1 x1.33333 x2	100.0%	86.8%
(3)	x0.5 to x2 by increments of 0.1	45.1%	12.5%

Table II: Scale classification for Chirp_1 using different sets of scales.

Correlation	Covariance	Homogeneity	MaxProb	Entropy	InvDiff	Dissimilarity	Inertia	Energy	Classification	
									Soft	Hard
X	x	x	x	x	X	x	x	x	100.0%	67.4%
	x	x	x	x	X	x	x	x	100.0%	67.3%
X		x	x	x	X	x	x	x	100.0%	69.4%
X	x		x	x	X	x	x	x	100.0%	67.4%
X	x	x		x	X	x	x	x	100.0%	67.3%
X	x	x	x		X	x	x	x	100.0%	67.3%
X	x	x	x	x		x	x	x	100.0%	67.3%
X	x	x	x	x	X		x	x	100.0%	74.3%
X	x	x	x	x	X	x		x	100.0%	69.4%
X	x	x	x	x	X	x	x		100.0%	67.3%
X									72.9%	42.2%
	x								100.0%	66.7%
		x							100.0%	67.3%
			x						93.8%	56.3%
				x					98.6%	66.7%
					X				34.7%	14.6%
						x			96.5%	58.3%
							x		95.8%	56.9%
								x	100.0%	69.4%
X	x	x		x	X	x	x		100.0%	67.3%

Table III: Comparison of scale classification results for chirp image Chirp_1 using reduced subsets of GLCM textural features.

Image	Orientation kernel size	Scale stationarity score	Reference pattern location	Scale estimation score /3	
D3	128x128	100%	Top left	2.5	
D4	64x64	95%	Top right	2.25	
D6	64x64	99%	Top right	2	
D11	128x128	100%	Top left	1.5	(b)
D13	64x64	95%	Top left	1.5	(a)
D15	64x64	95%	Top left	1.25	(c)
D16	64x64	90%	Top left	3	
D17	32x32	94%	Top right	3	
D18	64x64	99%	Top left	1.25	(b)
D20	64x64	99%	Top left	2.5	
D21	64x64	99%	Top left	3	
D23	64x64	99%	Top left	2	
D24	64x64	94%	Top right	3	
D28	64x64	97%	Top left	1.25	(b)
D29	64x64	94%	Top left	1	(a)
D33	64x64	88%	Top left	1.25	(a)
D34	64x64	99%	Bottom left	3	
D35	64x64	99%	Top left	3	
D36	64x64	99%	Bottom left	2.25	
D40	64x64	75%	Bottom left	1	(a)
D47	214x214	100%	Top left	2	
D51	214x214	84%	Bottom left	1	(d)
D53	64x64	100%	Top left	2.5	
D55	64x64	100%	Top left	1.5	(c)
D56	128x128	100%	Top left	2.5	
D57	64x64	100%	Top left	2	
D64	8x8	98%	Bottom left	2.25	
D65	128x128	98%	Top left	1.75	
D68	64x64	99%	Top left	3	
D74	32x32	100%	Top left	2.5	
D75	32x32	100%	Top left	1.5	(a)
D76	64x64	100%	Top left	2	
D77	64x64	99%	Top left	1.25	(c)
D79	64x64	95%	Top left	0	(e)
D80	64x64	100%	Top left	1.25	(e)
D82	64x64	91%	Top left	0	(e)
D83	64x64	94%	Top left	1.5	(c)
D84	64x64	100%	Top left	1.25	(c)
D86	64x64	98%	Top right	1.25	(c)
D87	64x64	100%	Top left	3	
D92	64x64	97%	Top right	0.75	(e)
D98	64x64	100%	Top left	2.25	
D101	128x128	100%	Top left	2.5	
D102	128x128	100%	Top left	3	
D103	16x16	100%	Top left	0.75	(c)
D104	16x16	100%	Top left	2	
D107	16x16	94%	Top right	1	(a)
D111	16x16	96%	Top left	2.5	

Table IV: Parameters and scale stationarity results for the selected Brodatz texture images.